Retrievals of Ozone in the Troposphere and Lower Stratosphere Using FTIR Observations over Greenland

Shima Bahramvash Shams, Von P. Walden, James W. Hannigan, and David D. Turner

***Abstract*—When retrieving geophysical parameters, it is advantageous to have an estimate of prior information that is based on observations with associated uncertainties, but this is often not possible. Long-term ground-based remote sensing measurements and the ozonesonde program at Summit Station, Greenland provide an opportunity to create a unique framework to retrieve atmospheric ozone using observationally-based prior information in the Arctic. This study investigates the potential of using the ground-based Polar Atmospheric Emitted Radiance Interferometer (P-AERI) to estimate ozone below 10 km. Downlooking or limb viewing sensors, such as those from satellites, lack sensitivity to the lower atmosphere; however, uplooking, ground-based instruments provide complementary information to satellite observations to improve trace gas estimates at lower atmospheric levels. MERRA-2 is a reanalysis product that integrates satellite information but also inherits their higher uncertainties at lower atmospheric levels. An observation-based climatology of the uncertainty in the MERRA-2 ozone dataset is estimated using ozonesondes launched at Summit Station. MERRA-2 shows high accuracy in the middle stratosphere, but larger uncertainties below 10 km. Retrievals that use spectral radiance measurements from the P-AERI improve estimates of ozone concentrations in the troposphere and lower stratosphere by using prior information from MERRA-2 and the climatology of MERRA-2 uncertainties as the covariance of the prior. Using ozonesonde observations from 2012 to 2017 at Summit Station, Greenland, the quality of the retrieved results is assessed. Comparisons show that retrieved partial columns reduce the bias of MERRA-2 ozone estimation below 10 km, and the average tropospheric ozone concentration is improved significantly.**

***Index Terms*—Atmospheric measurements, infrared radiometry, remote sensing.**

I. Introduction

GROUND-BASED remote sensing instruments, such as Fourier transform infrared (FTIR) spectrometers, can provide important information on atmospheric structure. One of the key advantages of ground-based infrared spectrometry compared to those measured from space or aircraft is the small contribution of reflectance and emission from the surface in the measurements. Using atmospheric radiance data over a broad spectral range from FTIR, a variety of atmospheric trace gases and meteorological parameters can be retrieved. In particular, ground-based atmospheric emitted radiance interferometer (AERI) instruments have been used in the analysis of cloud properties [1]-[6], trace gas retrievals such as CO [7], water vapor [8], [9], spectroscopic parameters of H_2O [10], [11], thermodynamic profiling [12]-[14], and radiative forcing associated with CO_2 [15] and CH_4 [16]. AERI instruments are sensitive to the middle to far infrared (3-21 micrometers), and as atmospheric emission instruments, they have an advantage over solar FTIR because they can make measurements in the absence of sunlight. Thus, they are well suited for operation at high latitudes where there is no sunlight for a significant portion of the year.

An AERI instrument was deployed in June 2010 at Summit Station, Greenland as part of the Integrated Characterization of Energy, Clouds, Atmospheric State, and Precipitation at Summit (ICECAPS) project [17] and is called the Polar AERI (P-AERI). In this study, we introduce a retrieval framework that takes advantage of the sensitivity of the P-AERI to atmospheric ozone in the lower atmosphere and the year-round operation of the P-AERI. Ozone retrievals from the P-AERI are then compared to an existing reanalysis dataset as well as ozonesonde profiles.

The accurate measurement of tropospheric and lower stratospheric ozone at high latitudes is important for a thorough understanding of stratospheric-tropospheric exchange [18]-[20], ozone variability, long-term trends in ozone, and the parameters and mechanisms that modulate lower-level ozone fluctuations [21]-[23]. Ozone is an important component of global climate [24]-[28]. Arctic ozone influences global circu-

Manuscript received October 15, 2021; revised X; accepted XX. Date of publication XXX; date of current version XXXX. This research was supported by NSF grants PLR-1420932, PLR-1414314, and NNA-1801764. This material is based upon work supported by the National Center for Atmospheric Research, which is a major facility sponsored by the National Science Foundation under Cooperative Agreement No. 1755088. J. Hannigan is supported under contract by the National Aeronautics and Space Administration (NASA). *(Corresponding author: Shima Bahramvash Shams.)*

S. Bahramvash Shams is with Washington State University, Pullman, WA 99164 USA and the National Center of Atmospheric Research, Boulder, CO 80301 USA (e-mail: s.bahramvashshams@wsu.edu, sshams@ucar.edu).

V. P. Walden is with Washington State university, Pullman, WA 99164 USA (e-mail:, v.walden@wsu.edu).

J. W. Hannigan is with the National Center of Atmospheric Research, Boulder, CO 80301 USA (e-mail: jamesw@ucar.edu).

D. D. Turner is with the National Oceanic and Atmospheric Administra- tion Global System Laboratory, Boulder, CO 80305 USA (e-mail: dave.turner@noaa.gov).

Color versions of one or more of the figures in this paper are available online at http://ieeexplore.ieee.org.

Digital Object Identifier YYYY.

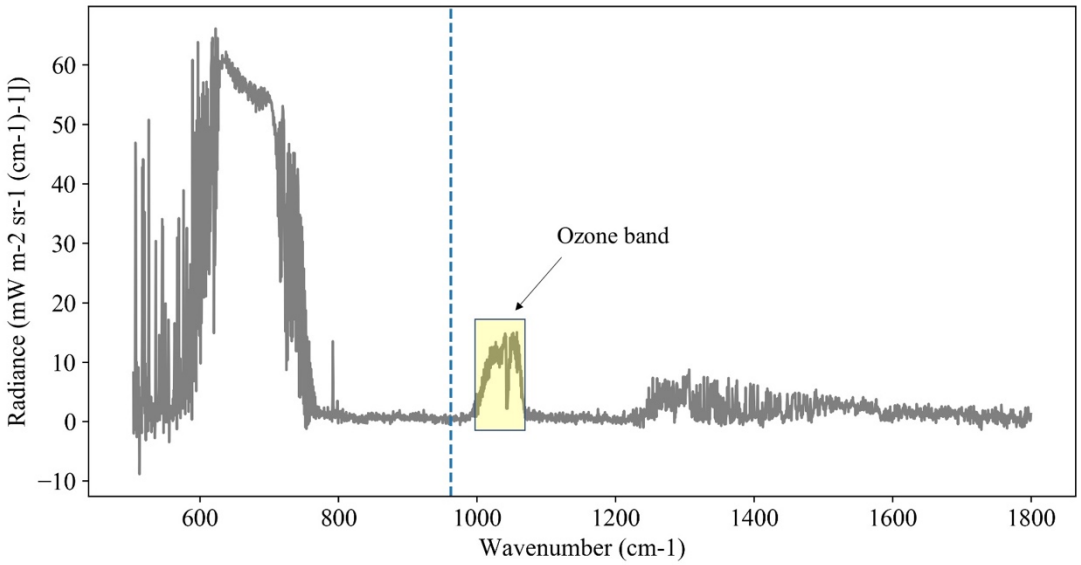

Fig.1. The spectral range and radiance of P-AERI channel 1. The spectral range of 995 to 1065 cm^{-1} is the ozone band and it is used for the retrieval. The radiance at 962.36 cm^{-1} is shown by the blue dash line and used to determine clear-sky conditions.

-lation, surface temperature, and tropospheric weather regimes [29]-[33]. Tropospheric ozone over the Arctic is impacted by anthropogenic pollutants from lower latitudes and stratospheric intrusions [34], [35]. Lower stratospheric ozone is mostly modulated by dynamical mechanisms and also impacted by ozone-depleting substances [36], [37]. Despite the consensus on the recovery of ozone in the middle stratosphere [38]-[40], trends of decreasing ozone have been reported within lower stratospheric layers [39], [41]-[43]. However, some model simulation studies contradict the decreasing trend because of the high interannual variability at lower stratospheric levels [44]. Many of the studies mentioned above [39]-[43] focused on the lower latitudes because of the complexity of dynamical mechanisms and their uncertainties and the sparsity of ozone observations in lower stratospheric/tropospheric layers over high latitudes. Thus, improving the estimation of tropospheric and lower stratospheric ozone at high latitudes is important for a complete understanding of ozone variations.

Reanalyses models assimilate observations, including satellite retrievals and meteorological measurements, to provide global coverage of atmospheric properties at fine temporal resolution. However, various uncertainties in the observations and assimilation methods, as well as uncertainties in the parameterizations of the physical processes within the modeling systems, contribute to uncertainties in the final reanalysis products [45], [46]. MERRA-2 reanalysis products have fine vertical resolution, global coverage, and agree well with observations at mid-stratospheric levels [47], [48]. Because of this, many studies have used MERRA-2 to study ozone in the middle stratosphere [48]-[50]. However, because of low sensitivity of spaceborne ozone estimations, MERRA-2 has larger uncertainties in the lower stratosphere and troposphere [47], [48]. The long record of P-AERI measurements (July 2010-April 2021) and ozonesonde profiles (2005-2017) at Summit Station motivate an exploration of the capabilities of the P-AERI to retrieve ozone that can be compared with ozonesonde measurements in the lower atmosphere at high northern latitudes.

Early attempts to retrieve ozone from emission FTIR used look-up tables and regression analysis to estimate ozone concentrations [51]. Previously, a combination of regression and physical retrieval was used to retrieve tropospheric column ozone from the surface to 300 hPa from an AERI using a case study from the mid latitudes [52]. In this study, tropospheric and lower stratospheric ozone is retrieved from emission FTIR spectra using the Optimal Estimation Method (OEM) [53]. MERRA-2 ozone profiles and the observation-based climatology of MERRA-2 uncertainties are used as the retrieval prior information and its uncertainty, respectively. The climatology of MERRA-2 uncertainties is estimated using 12 years of ozonesonde measurements at Summit Station. The climatological differences show good agreement between MERRA-2 and ozonesondes in the middle stratosphere, but larger uncertainties below 10 km. The larger magnitude of the prior uncertainty in the lower atmospheric layers puts more weight on P-AERI spectra in the OEM retrieval process, while the smaller uncertainties in the middle stratosphere put more weight on using the prior ozone information from MERRA-2. Thus, the retrieval framework focuses on the portion of the MERRA-2 ozone profile that has higher uncertainties. Moreover, the covariance among layers, as provided by the prior, provides additional constraints to limit the optimal solution and enable the retrieval to achieve a realistic result. To quantify the improvements of the retrieval results, coincident measurements of clear-sky P-AERI spectra and ozonesonde launches at Summit Station, Greenland are used.

In this study, the OEM is used to retrieve ozone from the P-AERI while being constrained by the climatology from the MERRA-2 product. The retrieved ozone columns are compared to ozonesondes and MERRA-2 from the ground to 10 km at Su-

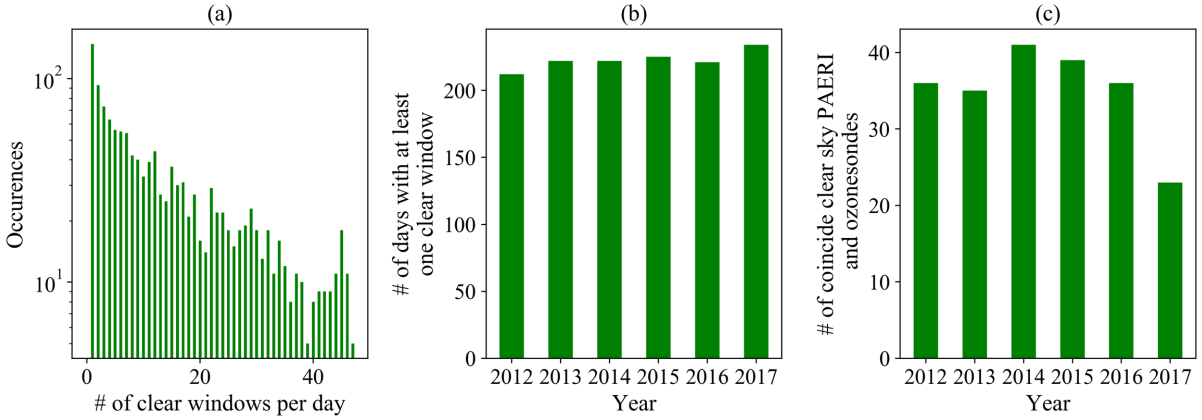

Fig. 2. Statistics of clear sky data. (a) the occurrences of clear sky windows (30 min) per day in all five and half years. (b) the number of days with at least one clear sky window for each year. (c) The number of coincident days of at least one clear sky window and an ozonesonde launch.

mmit Station, Greenland. Section 2 describes the datasets used in this study, including the P-AERI, the MERRA-2 reanalysis, and ozonesondes. In section 3, the retrieval methodology and procedures are presented. In section 4, the retrieved results and the details of the information content are discussed. The comparisons to ozonesondes are discussed in section 5. Section 6 presents the conclusions of this research study.

II. Data

This section provides a description of the datasets used in this study (P-AERI, MERRA-2, ozonesondes), including their uncertainties.

A. Polar AERI

Infrared spectra acquired using the P-AERI at Summit Station, Greenland (72°N, 39°W) are used to retrieve ozone. The P-AERI was designed and built by the Space Science and Engineering Center at the University of Wisconsin-Madison [54]-[56]. The P-AERI was deployed as part of the Integrated Characterization of Energy, Clouds, Atmospheric State, and Precipitation at Summit (ICECAPS) project in June 2010 [17]. The P-AERI measured downwelling infrared spectral radiance continuously at Summit Station until May 2021. The effective laser wavenumber during ICECAPS was determined to be 15799.33 cm^{-1}, which corresponds to a maximum optical path length of about 1.037 cm. The spectral range is 480 to 3000 cm^{-1} (3-21μm) with moderate unapodized spectral resolution of 0.48 cm^{-1} [54], [55], [57]. A representative example of a clear-sky measurement of downwelling infrared radiance by the P-AERI is shown in Fig 1. The radiance at 500-800 cm^{-1} corresponds to CO_2 and H_2O, 995-1065 cm^{-1} to the ozone bands, and 1200-1400 cm^{-1} to CH_4, N_2O, and H_2O. The radiometric calibration is determined using two well-characterized infrared sources [55]. The radiometric uncertainty of the P-AERI (3-sigma value) is less than 1% at ambient radiance [55]. The spectral calibration is approximately 1 ppm (standard deviation of +/- 0.014 cm^{-1}).

The P-AERI data from January 2012 to May 2021 have the best calibration (due to a temperature correction that was necessary for the infrared sources from July 2010 through December 2011). In this study, ozone retrievals are performed for 5.5 years from January 2012 to July 2017. The end of the study period corresponds to the termination of the ozonesondes program at Summit Station, which provides the comparison data to assess the quality of retrievals. The P-AERI measurements are taken approximately every 30 seconds year-round for a total of about 3300 spectra each day. Continuous radiance measurements is an advantage of using P-AERI observations for ozone retrievals. When clouds are present, they contribute radiance in the 9.6-micron ozone band, so it is important to determine periods of clear-sky conditions to achieve high-quality ozone retrievals. The mean and standard deviation of a 30-min rolling window of the radiance at 962.36 cm^{-1} is used to determine clear-sky conditions because of the low gaseous optical depth at this wavenumber, which make it very sensitive to the emission from overlying clouds. Even very small, condensed water amounts can greatly increase the radiance observed in the 11 μm window [58] and, because clouds are seldom spatially uniform, they introduce a temporally-varying signal that can be easily identified using thresholds on the mean and standard deviation of the rolling window. Because the infrared emission from atmospheric gases varies slowly with seasons [due to changes in atmospheric temperature and gas concentrations (e.g., water vapor)], thresholds are set for the mean and standard deviation of clear-sky conditions for each month. To reduce the uncertainty in the spectral radiances (and to increase the signal-to-noise ratio), the clear-sky infrared spectra are averaged over 30-min time periods. The statistics of clear-sky spectra are shown in Fig. 2. Most days with clear sky have only a single period that is cloud-free for more than 30-minutes. Most clear days have a single 30-min period of clear skies, but some days have more clear periods. Using the monthly thresholds, we have identified more than 200 days with at least one 30-min period of clear sky conditions per year. The retrievals performed in this study are also limited to times that have coincident ozonesonde profiles that are used to assess the uncertainties of the retrieval. For days with multiple 30-min clear sky periods, the averaged spectra of the nearest clear period to the coincident ozonesonde are

selected for this study. These criteria resulted in a total of 201 cases, with more than 30 cases for each year (except in 2017, which only had 6 months of ozonesonde data).

B. MERRA-2

Using the Goddard Earth Observing System (GEOS) version 5 general circulation model and the Gridpoint Statistical Interpolation (GSI) [59], the Modern-Era Retrospective Analysis for Research and Application, version 2 (MERRA-2) reanalysis products are created by NASA's Global Monitoring and Assimilation Office (GMAO) [46], [60] (available at GES DISC; http://disc.sci.gsfc.nasa.gov) at a spatial resolution of $0.5^{\circ} \times 0.625^{\circ}$. Various satellite data products, including the Solar Backscatter Ultraviolet Radiometer (SBUV), Ozone Monitoring Instrument (OMI), and the Aura Microwave Limb Sounder (MLS) are integrated into the MERRA-2 ozone estimation [46], [47].

When using any reanalysis model such as MERRA-2, uncertainties in the model physics, data assimilation methods, and observations can cause uncertainties in the products [45]. The global average of MERRA-2 evaluations has a standard deviation of 5% in the ozone concentrations in the middle to upper stratosphere (10 to 30 km) [47]. However, the uncertainties increase at lower altitudes with standard deviations of 20%-24% in the global estimation in the lower stratosphere and troposphere [47]. Previous MERRA-2 validation using ozonesondes in the middle to upper stratospheric layers over the high latitudes during highly altered circulation of sudden stratospheric warmings showed good agreement with observations with standard deviation of 4% to 7% [48]. However, the tropospheric and lower stratospheric layers show a mean difference of 5% to 18% with a standard deviation of 15% to 26% [48].

C. Ozonesondes

Ozonesondes provide an in situ measurement of the vertical profile of ozone using electrochemical concentration cells (ECCs) [61]. The response time and ascent rate of the ozonesonde balloons yield a vertical resolution of around 100 m. The measured ozone is expected to have an uncertainty of 3%-5% [61]-[64]. The fine vertical resolution and quality of measurements make ozonesondes an independent source for ozone validation [34], [48], [65], [66] as well as a direct source for monitoring ozone [22], [67]-[70].

In this study, we use ozonesonde profiles from Summit Station, Greenland (72°N, 39°W) to create a climatology of MERRA-2 uncertainty and as a source of validation. The ozonesonde program at Summit Station was started by the Global Monitoring Laboratory (GML) of the National Oceanic and Atmospheric Administration (NOAA) in February 2005 and continued until the summer of 2017. The ozonesonde data is available from NOAA's Earth System Research Laboratory. More details of the Summit Station ozonesondes and analysis can be found in previous studies [22], [71].

III. Methods

Retrieving trace gas information from observed infrared spectra is an ill-posed problem. Different approaches can be used to solve this problem. The OEM [72], [73] is based on Bayes theorem to retrieve a rigorous and physically-based quantity from measured spectra. The basic equation of y=Kx+e relates the state vector, x (unknowns), to the measurement vector, y. In this case, the downwelling spectral radiance measurement is y, the state vector (x) is the ozone concentration profile, and e is an error term. K is the derivative of a forward model (F) with respect to the state vector, $\frac{dF(x)}{dx}$, and is called the Jacobian matrix or kernel. In passive remote sensing retrievals, the forward model is a radiative transfer model (RTM). The forward model in ground-based remote sensing retrieval uses spectroscopic information, along with the concentration of atmospheric trace gases, temperature, and pressure on a vertical grid, to estimate the downwelling radiation at the surface. Considering all of the uncertainties in the measurements and assuming Gaussian distributions for the variables, OEM simplifies the Bayes theorem to achieve an optimal estimation of the state vector from:

$$\hat{x}_{n+1} = x_a + (K^T S_e^{-1} K + S_a^{-1})^{-1}\{K^T S_e^{-1}[y - F(\hat{x}_n) + \mathrm{K}(\hat{x}_n - x_a)]\} \quad (1)$$

$$\mathrm{G}=(K^T S_e^{-1} K + S_a^{-1})^{-1} K^T S_e^{-1} \quad (2)$$

where n is the number of iterations, $\hat{x}$ is the expected state vector, x_a is the prior, S_e is the covariance of measurement uncertainties, and S_a is the covariance of prior information. OEM addresses the inverse problem by iteratively updating the posterior probability density function (PDF) of the state vector. A characteristic metric of the retrieval is the averaging kernel (A), also known as the resolution matrix, which is defined as A=GK. Important details of the information content associated with a retrieval can be derived from the averaging kernel, including the vertical resolution of the retrieval and the degrees of freedom of the signal (DOFS). DOFS for the retrieval is estimated from the trace of the matrix A and indicates the level of detail of the information that can be retrieved from the spectra.

In this study, the Spectra FITting Algorithm, version 4 (SFIT4), is used to retrieve the ozone profile. SFIT4 is one of the algorithms that apply the OEM to infrared spectra [74]. SFIT has been used to retrieve ozone and other trace gases from solar FTIR sensors [65], [75], [76]. The embedded radiative transfer model in SFIT4 has shown good agreement when compared to the Line By Line Radiation Transfer Model (LBLRTM) [74]. The spectroscopic database from HITRAN 2008 is used in the retrieval [77]. The convolution of spectra calculated by SFIT4 with the P-AERI instrument line shape (ILS) creates synthetic spectra that have similar spectral characteristics to those measured by the P-AERI. Three-hourly temperature and ozone profiles from MERRA-2 and monthly profiles of water vapor and CO_2 from the Whole Atmosphere Community Climate Model WACCM4 [78] are used as the prior information for retrievals in this study.

The P, Q, and R branches of $\nu 3$ vibrational-rotational modes of ozone molecules exhibit emission (and absorption) near 9.6 micrometers [79], creating a broad spectral feature at mid spectral resolution spectra from about 995 to 1070 cm^{-1}. This spectral range is used for the ozone retrievals in this study and is shown in Fig. 1. To account for other gases in the retrieval spectral range, the column amount of CO_2 (with 0.01% Sa, corr-

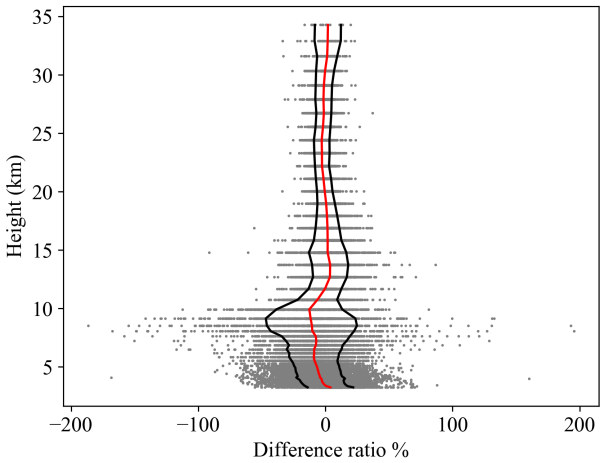

Fig. 3. The profile of difference ratios of MERRA-2 ozone mixing ratio (computed as (MERRA-2 minus ozonesonde)/ozonesonde). The mean of differences is shown in the red line. The mean+/- standard deviation difference ratio is shown as the black line.

espond to 4 ppmv) and water vapor (with 0.25% Sa, correspond to 20 ppmv at surface level), are considered in the retrieval. MERRA-2 ozone profiles are used as the ozone prior information.

To estimate the uncertainty of the prior ozone information, the long record of ozonesondes program at Summit Station are compared to MERRA-2 ozone estimations. These comparisons as shown in Fig. 3, including the difference ratio [(MERRA-2 minus ozonesonde)/ozonesondes], mean, and standard deviation of differences. The uncertainties are estimated using the entire dataset of ozonesondes from Summit from 2005 to 2017. The climatology of MERRA-2 ozone uncertainty is estimated as the covariance of differences in comparison to ozonesonde and is used as the covariance of the prior as shown in Fig. 4a. By considering the level-to-level interdependency of uncertainties in MERRA-2 (non-diagonal elements of Sa), this framework adds further constraints based on the observations so that the retrieval achieves a more realistic result.

To allow the retrieval to consider the full range of uncertainties in the OEM process, three times the standard deviations are used as the Sa (hereafter 3σ) at each level. The climatology of MERRA-2 uncertainties (Sa) can be summarized as: 1) from ground to 7 km, 3σ allows 50% change of ozone at each level, and the dependency among layers has the highest spatial extent in these layers; 2) from 7 to 10 km, 3σ allows ~90% ozone variations at these levels with a high degree of dependency to nearby layers in the retrieval process; and 3) above 10 km, the dependency of uncertainties among layers is diminished, and the diagonal values show that 3σ occurs from ~ 20% and quickly decreases with altitude down to about 5% above 15 km. The variability in the vertical uncertainties reflect the high quality of mid-stratospheric ozone in MERRA-2 and the large uncertainties of MERRA-2 below 10 km and are consistent with previous studies [47], [48]. The observation-based Sa allows the retrieval to weight the P-AERI spectral information more heavily to determine the optimal ozone estimate below 10 km, while above 15 km, the retrieval mostly relies on the prior (MERRA-2). Between 10-15 km, the retrieval combines information from both sources.

Another essential component of OEM is the requirement of a measurement uncertainty estimate S_e. S_e has two main components [53] ,[80]: S_y (the covariance of measured radiance) and S_b (the covariance of the forward model and associated parameters). The random noise of 0.4 mW/(m^2 sr cm^{-1}) is the estimated uncertainty of the P-AERI radiance for a 30-s sky view in the 995-1070 cm^{-1} region. Because the P-AERI spectra are averaged for 30 minutes during clear skies, the spectral noise reduces by the square root of the number of averaged spectra. The covariance of the parameters in the forward model and the spectroscopic dataset have a significant contribution to the covariance of errors (S_e) [13], [80]. However, quantifying S_b, which translates to quantify the uncertainties of all of the absorption line parameters, would require extensive work and has not been done. Thus, a simplified estimation has been applied [13]. In this study to prevent unrealistic fluctuations of retrieved data by introducing exaggerated low error covariance [13], the final estimation of error covariance (S_e) for ozone retrieval is estimated to be 0.16 mW^2/(m^4 sr^2 cm^{-2}) [whereas if we assumed Sb = 0, the estimate of the error covariance used in Se would be 0.0025 mW^2/(m^4 sr^2 cm^{-2})].

IV. Retrieval Information Content

To assess the retrieval performance, retrievals in clear sky situations were first evaluated using information provided by the retrieval algorithm itself. To understand the information content of the retrievals, different aspects of the retrieval will be discussed including: the spectral fit and contribution of each trace gas, the Jacobian matrix, the average kernel profiles, DOFS, and the posterior covariance matrix. Fig. 5 shows the observed spectral radiance, simulated radiances (fitted), the residual of fitted radiances, and the contribution of ozone, CO_2, and water vapor to the fit spectra in 995 to 1070 cm^{-1} spectral region for cases on 26 July 2012 (panel (b)) and 12 December 2012 ((panel (d)). Comparison of the spectral signatures on summer and winter days shows the importance (and the interference) of water vapor on the observed radiance during a summer day at Summit Station. The largest interfering signatures of water vapor are between 1010 to 1020 cm^{-1} and 1028 to 1030 cm^{-1} during humid spring/summer days (panel (b), Fig. 5). From 1030 to 1060 cm^{-1}, CO_2 and water vapor both contribute to the fitted spectra. The residual of the fitted spectra and the observed radiance have mostly random structure and are below the radiance random noise limit of 0.4 mW/(m^2 sr cm^{-1}) as shown in panel (a) and (c) of Fig. 5.

The averaged Jacobian matrix of all cases indicates the vertical sensitivity of the retrieval at each wavenumber and is shown in Fig. 6. The Jacobian matrix has large values around 17 km and has maximum values between 1010 to 1040 cm^{-1} and 1045 to 1060 cm^{-1}. The vertical sensitivity of the Jacobian matrix is impacted primarily by the vertical structure of the ozone profile up to 17 km as the ozone profile is fairly uniform from the ground to ~7 km (the climatological tropopause at Summit Station), but then rapidly increases. Although the maximum peak of ozone concentration is higher in the middle

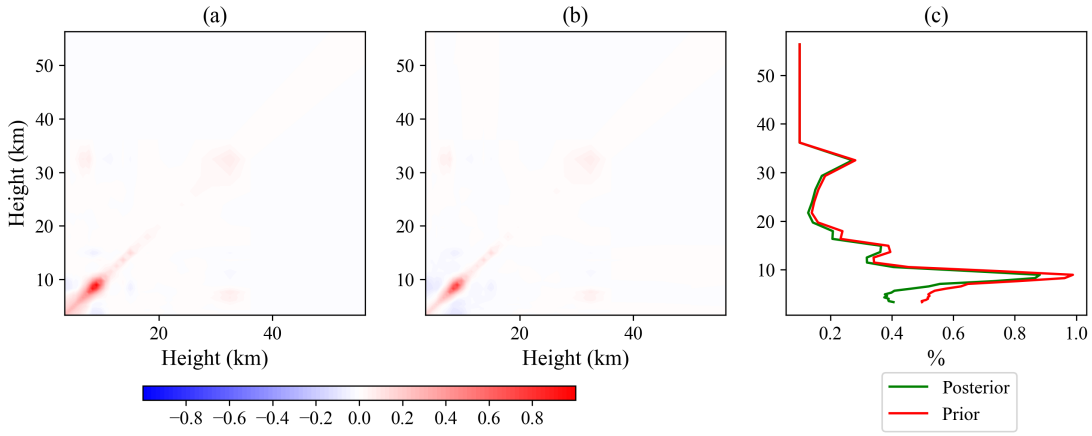

Fig. 4. The covariance of a priori and posterior. Panel (a) the covariance of Sa which is based on 3 standard deviations of MERRA-2 ozone covariance of uncertainties in comparison to ozonesondes. Panel (b) shows the posterior covariance of retrieval. Panel (c) shows the root square of diagonal element of covariance matrix for both prior and posterior by height.

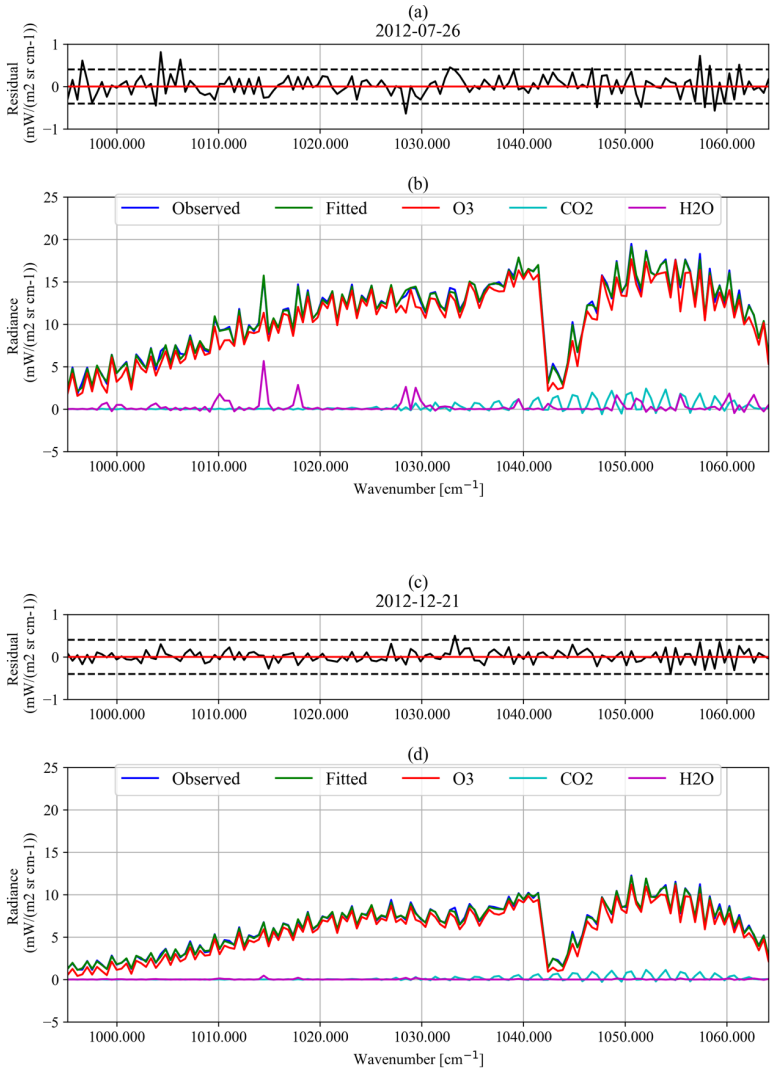

Fig. 5. observed radiance (blue), fitted synthetic radiance (green), the radiance contribution of ozone (red), CO2 (aqua), and H2O (pink), and the residual in the spectral range of retrieval in 995 to 1065 cm^{-1}. The upper panels show the humid summer day 2012-07-26 with a significant contribution of water signature in the spectra and the lower panel the dry winter spectra from 2012-12-21. Black dash lines in the residual panel indicate plus and minus the spectral noise level ($\pm$0.4 $mW/(m^2\ sr\ cm^{-1})$).

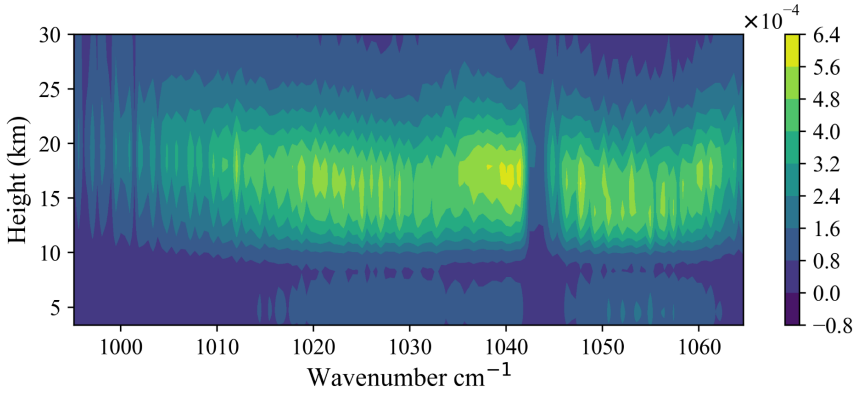

Fig. 6. The average Jacobian matrix in unit of radiance divided by O3 mixing ratio for all retrieved cases.

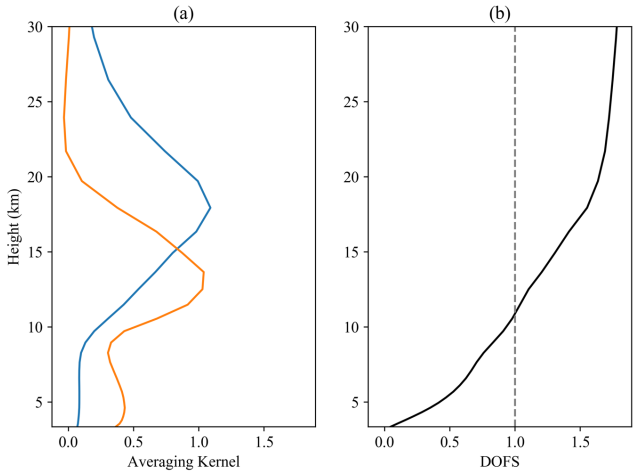

Fig. 7. The mean of averaging kernel profiles and DOFS of all retrieved cases. (a) average kernel profiles, orange line shows the sensitivity to the lower atmosphere and the blue line corresponds to the middle stratospheric layers (b) the cumulative profile of DOFS.

stratosphere, the sensor sensitivity decreases above 17 km, which

reduces the ability of the P-AERI to detect ozone above this height. Because MERRA-2 provides 3-hourly ozone profiles that agree well with ozonesondes in the middle stratosphere, the focus of this study is to retrieve accurate ozone concentrations below 10 km where the Jacobian matrix shows sensitivity between 1015 to 1042 cm^{-1} and 1045 to 1062 cm^{-1}.

The posterior covariance matrix, defined as $(K^T S_e^{-1} K + S_a^{-1})^{-1}$, is reduced compared to the covariance of the prior, as is shown in Fig. 4b. The root square of diagonal elements of the posterior covariance, representing the uncertainty in the expected state vector, are decreased compared to the Sa. This reduction is more pronounced from surface to 7 km as is shown in Fig. 4c. The level-to-level covariance from the surface to 7 km is dramatically reduced and some reduction is evident in the 7-10 km layer. The mean averaging kernel profiles and DOFS are shown in Fig. 7. The averaging kernel indicates the smoothing of the true state vector based on the sensitivity of the sensor. The summation of the rows of the averaging kernel (until it reaches value of one) shows the possible retrieved partial columns based on the sensitivity of the sensor [73]. As shown in Fig. 7a, the averaging kernels show two profiles, one sensitive to the middle stratosphere and the other sensitive to the lower stratosphere and troposphere. The cumulative DOFS reaches 1 by around 10 km, thus, one partial column of ozone can be retrieved below 10 km. The time series of DOFS for two partial column ozone (PCO) values from the surface to 10 km and from 10 to 30 km are shown in Fig. 8. The seasonal variability in the DOFS for the two levels is evident in Fig. 8. Below 30 km, the sensitive altitude range of the sensor, a higher molecular density of ozone creates a stronger radiance signature in the measured P-AERI spectra and, consequently, increases the information content. The seasonal variability of the DOFS for PCO values exhibits the same cycle as ozone; the middle stratospheric ozone reaches a maximum during spring caused by the residual circulation, while the tropospheric and lower stratospheric ozone are impacted by photolysis and, therefore, peak during summer. More discussion on the seasonal cycle of ozone and the associated drivers at northern high latitudes (including Summit Station) is found in a previous study [22].

V. Comparison With Ozonesondes

In this section, the retrievals are compared with ozonesonde data that were obtained within 24 hours of clear-sky P-AERI radiance measurements. Summit Station is a high altitude (3250 m), remote site that is far from sources of tropospheric ozone precursors at high northern latitudes. Due to the consistent presence of sunlight during polar days and the lack of sunlight during polar nights, diurnal variations are small in tropospheric ozone concentrations. Thus, to have more robust statistics, the ozonesondes within a day of P-AERI retrieval provide an adequate set of validation measurements. However, more than 63% of the ozonesondes and clear-sky P-AERI measurements are less than 5 hours apart, while less than 10% of the cases have a time difference greater than 15 hours. Moreover, there is no significant correlation between the time difference between the P-AERI and ozonesonde observations and the differences in concentrations between the P-AERI retrievals and ozonesondes.

Fig. 9 shows the PCO difference between the retrievals (green) and prior from MERRA-2 (red) relative to the ozonesondes. Fig. 10 shows 16 examples of retrieved ozone to illustrate how the retrieved ozone compares to the MERRA-2

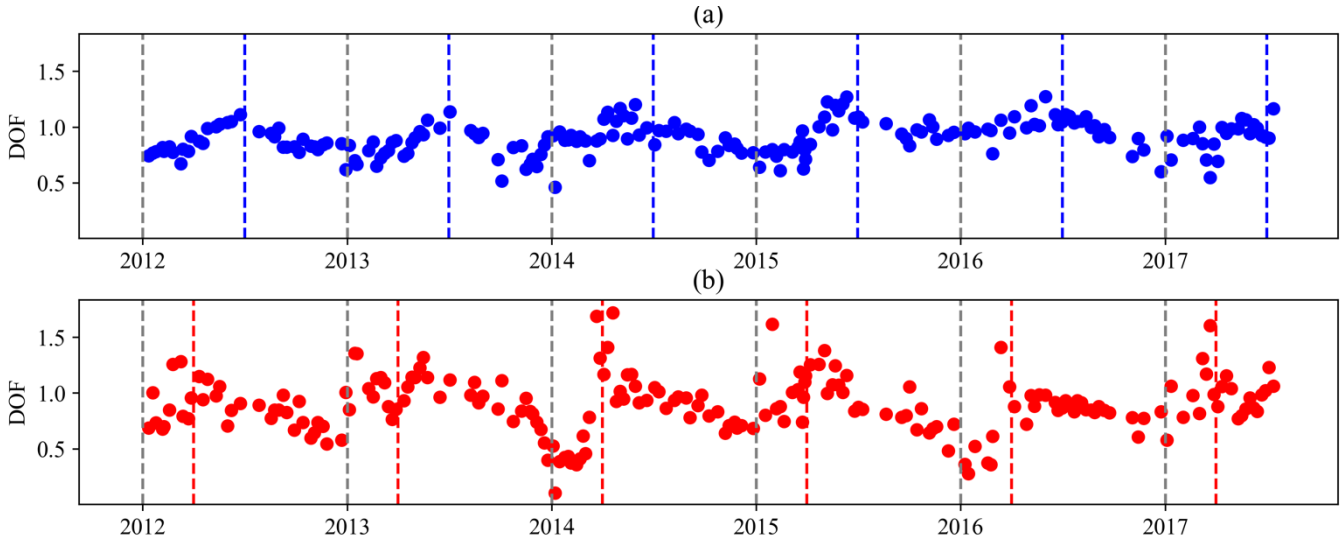

Fig. 8. Time series of DOFS and the impact of seasonal cycle on DOFS. (a) Ground to 10 km, (b) 10 to 30 km. Blue and red dash lines are plotted on July 1st and April 1st of each year, respectively.

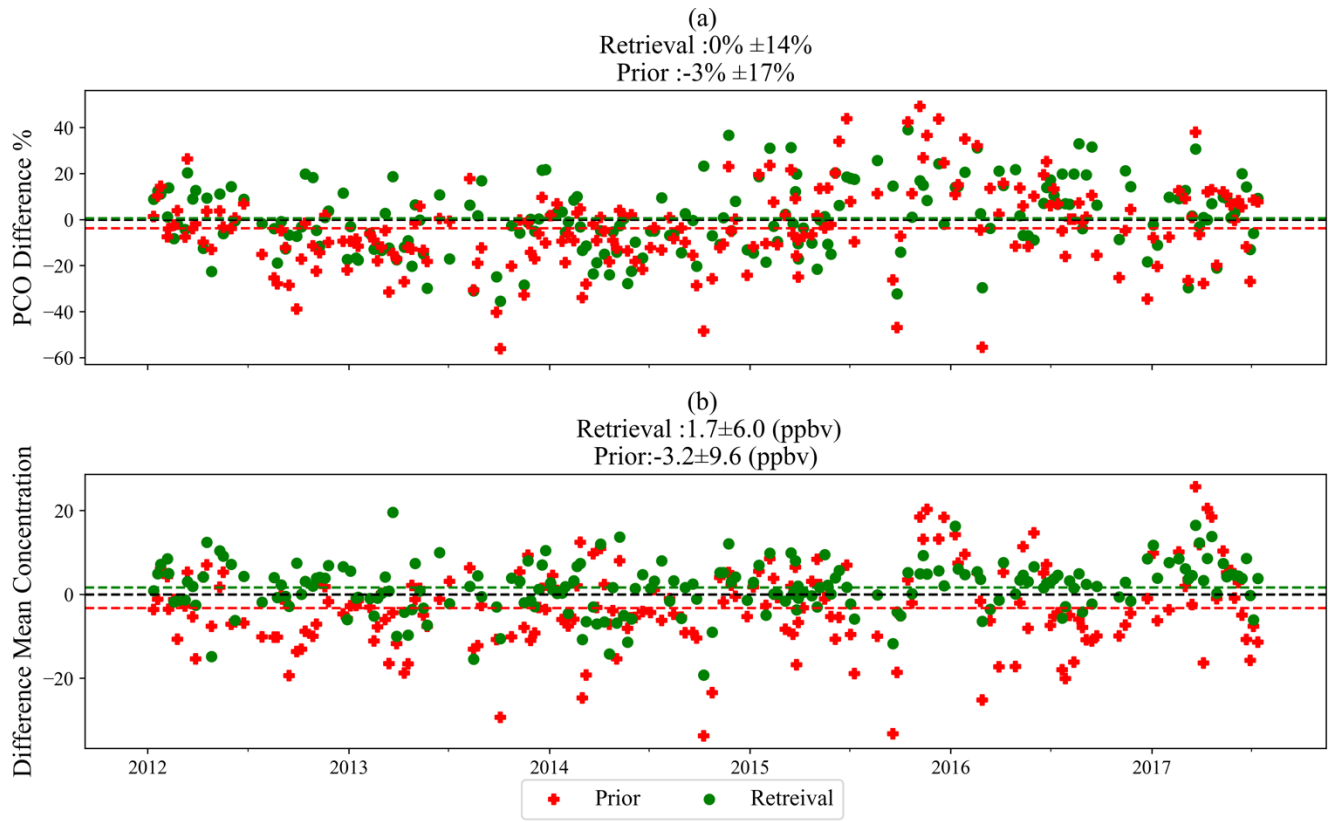

Fig. 9. The comparison of the retrieval and a priori to the independent ozonesonde observation. (a) PCO comparison from ground to 10 km, the difference ratios are (x-PCO minus ozonesondes-PCO)/ozonesondes-PCO*100, x be retrieved or the prior. (b) Comparison of mean ozone concentration up to 7 km (where ozone profile is fairly uniform), differences are x- ozonesonde mean concentrations. The average difference ratio and difference concentrations are shown by dash lines. The green color is assigned to the comparisons corresponding to retrievals and red to the prior. The black dash line shows the zero line, and the mean and standard deviations are reported on top of each panel.

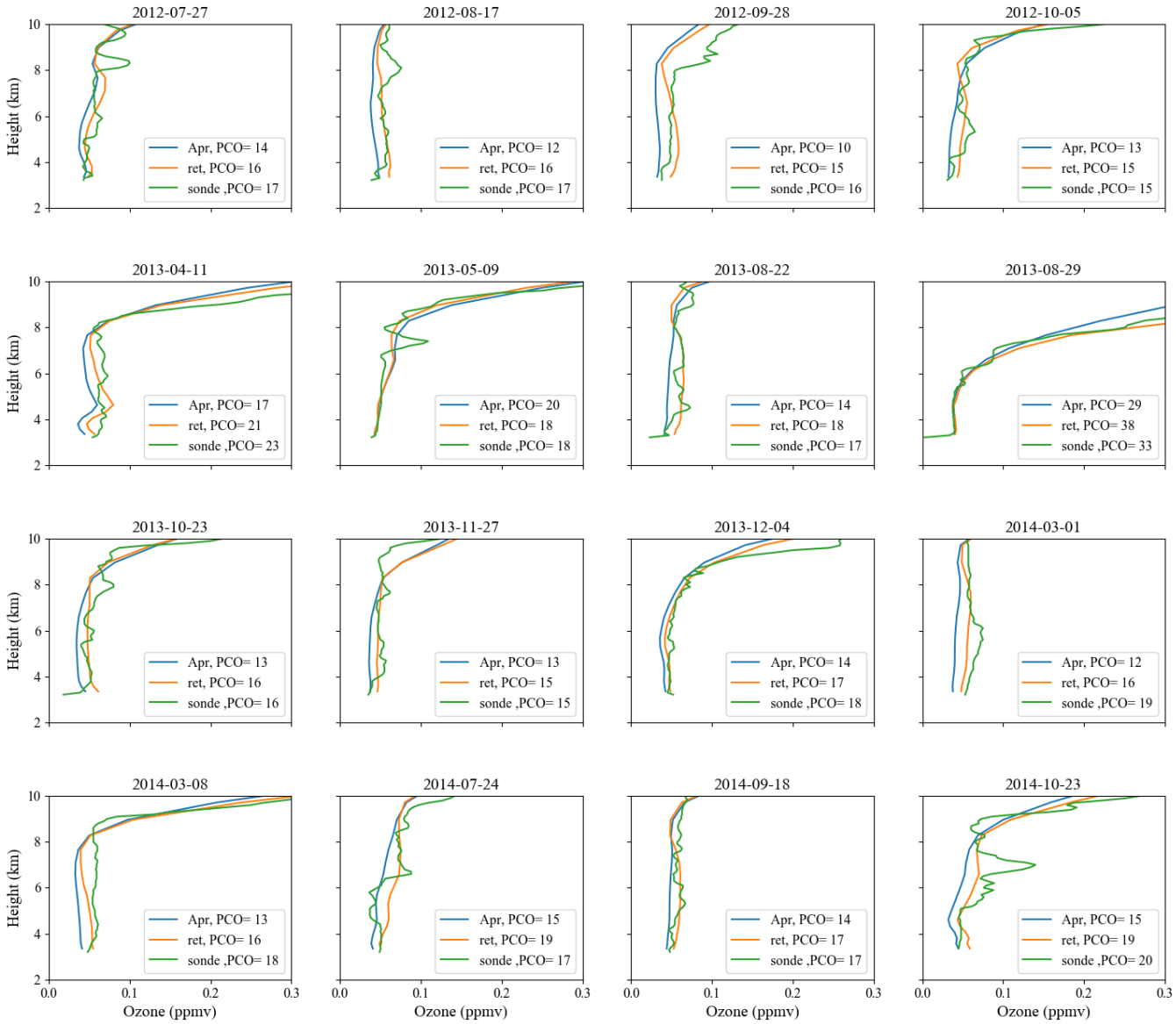

Fig. 10. The tropospheric/lower stratospheric ozone profile. Sixteen cases of retrieval elaborate the tropospheric/lower stratospheric ozone profile of the prior, final retrieval, and ozonesondes in blue, orange, and green lines, respectively. The associated PCO of ground to 10 km is reported in the lower right of each plot.

prior and ozonesondes. Fig. 9a shows the difference ratio of the PCO from surface to 10 km from ozonesondes subtracted from retrieved PCO and divided by ozonesonde's PCO multiplied by 100; the same quantity is also shown using the prior information. The retrieved PCO improved the bias in the prior and reduced the standard deviation from 17% to 14%. Because the estimation of molecular density depends on temperature, we also looked at mean ozone concentrations for tropospheric layers to focus solely on ozone estimates. To consider the fairly uniform ozone profile concentration from surface to 7 km (climatological tropopause at Summit station; evident in Fig. 10), the vertical mean concentration of ozone (surface to 7 km) is compared to ozonesondes. The mean ozone concentration bias from the surface to 7 km is 1.7±6 ppbv, which improves the original bias (-3.2± 9.6 ppbv) between the prior and ozonesondes, shown in Fig. 9b. It is important to mention that, because of the moderate spectral resolution of the P-AERI, this emission FTIR is unable to vertically resolve the detailed structures of ozone profile. Thus, Fig. 10 illustrate that final retrieval profiles have reasonable structure and improvement is not accomplished through random fluctuations. To further illustrate the improvement from the retrieval, the probability density functions of differences between the retrieval and MERRA-2 relative to the ozonesondes is shown in Fig. 11. The significant improvement of the average tropospheric ozone that improves the bias below 10 km, is evident in Fig. 11. The retrieval is most successful in improving the tropospheric ozone from surface to 7 km compared to surface to 10 km, which is due to the higher sensitivity of the FTIR in this region as seen in both the averaging kernel and the Jacobian matrix.

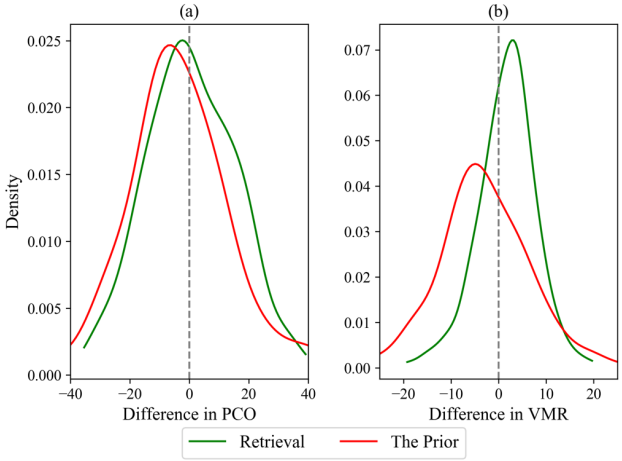

Fig. 11. The probability density functions of differences between retrieval and ozonesondes (green) vs MERRA-2 and ozonesondes (red). (a) for the PCO from the ground to 10 km, (b) for average mixing ratio from the ground to 7 km.

VI. Conclusion

The improved estimation of tropospheric and lower stratospheric ozone concentrations is critical to gain further knowledge of tropospheric-stratospheric ozone exchange, the impact of anthropogenic pollutants on ozone, ozone transport mechanisms, and the influence of climate change and ozone. Reanalysis models such as MERRA-2 integrate a variety of satellite measurements and meteorological data to provide ozone estimates with daily or sub-daily temporal resolution around the globe. However, despite good agreement of MERRA-2 ozone estimates with observation in the middle stratosphere, larger uncertainties exist in the lower stratosphere and troposphere.

The long record of emission FTIR measurements obtained by the Polar Atmospheric Emitted Radiance Interferometer (P-AERI) since 2010 and the ozonesonde program between 2005 to 2017 at Summit Station, Greenland, provides a unique opportunity to investigate the capability of emission FTIR to improve the ozone estimates of the lower stratosphere and troposphere at high northern latitudes and to quantify the comparisons to MERRA-2.

MERRA-2 ozone profiles are used as the first guess of the retrieval process. The retrieval process utilizes the climatological MERRA-2 uncertainties to focus the ozone retrieval through the optimal estimation method on altitudes that are uncertain. Using ozonesondes, the climatological uncertainties of MERRA-2 at Summit Station are estimated and are used as an observational-based covariance matrix of the prior in the retrieval process. The retrieval weights the MERRA-2 product heavily in the middle stratosphere where uncertainties are low and the P-AERI spectra more heavily in lower atmosphere layers where MERRA-2 uncertainties are high. The off-diagonal elements of the covariance matrix, which show the level-to-level dependency of uncertainties in MERRA-2 ozone dataset, introduce extra constraints to the ill-posed problem and lead to more realistic results.

The retrieved ozone from the ground to 10 km reduces a 3% underestimation of the ozone partial column in the MERRA-2 compared to ozonesondes and decreases the standard deviation. Moreover, the mean concentration of tropospheric ozone, from the ground to 7 km, is significantly improved, while the standard deviation is decreased from 10 ppbv to 6 ppbv.

In conclusion, emission FTIR with moderate spectral resolution can be used to improve lower atmospheric ozone estimates in the Arctic. Considering the network of ozonesonde measurements globally, the observation-based estimate of S_a can be used in a variety of locations and latitudes. Having an extended FTIR network could expand the findings of this study to the global scale to improve monitoring of ozone profiles below 10 km. Moreover, integration of the emission and solar FTIR as assimilation data for reanalysis models such as MERRA-2 could improve ozone datasets globally.

Acknowledgment

We acknowledge NASA's Global Monitoring and Assimilation Office (GMAO) for providing the Modern-Era Retrospective analysis for Research and Applications, Version 2 (MERRA-2). We acknowledge the Ozone and Water Vapor Group at the Earth System Research Laboratory of the National Oceanic and Atmospheric Administration for use of the ozonesonde data and the science technicians at Summit Station, Greenland for launching the ozonesondes. We thank Jason English (NOAA GSL) for providing comments on an early version of this manuscript.

References

[1] G. G. Mace, T. P. Ackerman, P. Minnis, and D. F. Young, "Cirrus layer microphysical properties derived from surface-based millimeter radar and infrared interferometer data," *Journal of Geophysical Research*, vol. 103, no. 18, pp. 23207–23216, Sep. 1998.

[2] A. Mahesh, V. P. Walden, and S. G. Warren, "Ground-Based Infrared Remote Sensing of Cloud Properties over the Antarctic Plateau. Part I: Cloud-Base Heights.," *Journal of Applied Meteorology*, vol. 40, no. 7, pp. 1265–1278, Jul. 2001.

[3] A. Mahesh, V. P. Walden, and S. G. Warren, "Ground-Based Infrared Remote Sensing of Cloud Properties over the Antarctic Plateau. Part II: Cloud Optical Depths and Particle Sizes.," *Journal of Applied Meteorology*, vol. 40, no. 7, pp. 1279–1294, Jul. 2001.

[4] M. S. Town, V. P. Walden, and S. G. Warren, "Spectral and Broadband Longwave Downwelling Radiative Fluxes, Cloud Radiative Forcing, and Fractional Cloud Cover over the South Pole.," *J. Climate*, vol. 18, no. 2, pp. 4235–4252, Oct. 2005.

[5] D. D. Turner, "Arctic Mixed-Phase Cloud Properties from AERI Lidar Observations: Algorithm and Results from SHEBA.," *Journal of Applied Meteorology*, vol. 44, no. 4, pp. 427–444, Apr. 2005.

[6] C. J. Cox, V. P. Walden, G. P. Compo, P. M. Rowe, M. D. Shupe, and K. Steffen, "Downwelling longwave flux over Summit, Greenland, 2010-2012: Analysis of surface-based observations and evaluation of ERA-Interim using wavelets," *J. Geophys. Res.*, vol. 119, no. 2, p. 12, Nov. 2014.

[7] L. Yurganov, W. McMillan, C. Wilson, M. Fischer, S. Biraud, and C. Sweeney, "Carbon monoxide mixing ratios over Oklahoma between 2002 and 2009 retrieved from Atmospheric Emitted Radiance Interferometer spectra," *Atmos. Meas. Tech.*, vol. 3, no. 5, pp. 1319–1331, 2010.

[8] D. C. Tobin, F. A. Best, P. D. Brown, S. A. Clough, R. G. Dedecker, R. G. Ellingson, R. K. Garcia, H. B. Howell, R. O. Knuteson, E. J. Mlawer, H. E. Revercomb, J. F. Short, P. F. W. van Delst, and V. P. Walden, "Downwelling spectral radiance observations at the SHEBA ice station: Water vapor continuum measurements from 17 to 26μm," *J. Geophys. Res.*, vol. 104, no. D, pp. 2081–2092, Jan. 1999.

[9] P. M. Rowe, V. P. Walden, and S. W. A. optics, "Measurements of the foreign-broadened continuum of water vapor in the 6.3 μm band at− 30° C," *Applied Optics*, vol. 45, no. 18, pp. 4366–4382, 2006.

[10] D. D. Turner, D. C. Tobin, S. A. Clough, P. D. Brown, R. G. Ellingson, E. J. Mlawer, R. O. Knuteson, H. E. Revercomb, T. R. Shippert, W. L. Smith, and M. W. Shephard, "The QME AERI LBLRTM: A Closure Experiment for Downwelling High Spectral Resolution Infrared Radiance.," *Journal of Atmospheric Sciences*, vol. 61, no. 2, pp. 2657–2675, Nov. 2004.

[11] E. J. Mlawer, V. H. Payne, J. L. Moncet, J. S. Delamere, M. J. Alvarado, and D. C. Tobin, "Development and recent evaluation of the MT_CKD model of continuum absorption," *Philosophical Transactions of the Royal Society A: Mathematical*, vol. 370, pp. 2520–2556, Jun. 2012.

[12] W. F. Feltz, W. L. Smith, H. B. Howell, R. O. Knuteson, H. Woolf, and H. E. Revercomb, "Near-Continuous Profiling of Temperature, Moisture, and Atmospheric Stability Using the Atmospheric Emitted Radiance Interferometer (AERI).," *Journal of Applied Meteorology*, vol. 42, no. 5, pp. 584–597, May 2003.

[13] D. D. Turner and W. G. Blumberg, "Improvements to the AERIoe Thermodynamic Profile Retrieval Algorithm," *IEEE J. Sel. Top. Appl. Earth Observations Remote Sensing*, vol. 12, no. 5, pp. 1339–1354, May 2019.

[14] D. D. Turner and U. Löhnert, "Ground-based temperature and humidity profiling: combining active and passive remote sensors," *Atmos. Meas. Tech.*, vol. 14, no. 4, pp. 3033–3048, Apr. 2021.

[15] D. R. Feldman, W. D. Collins, P. J. Gero, M. S. Torn, E. J. Mlawer, and T. R. Shippert, "Observational determination of surface radiative forcing by CO2 from 2000 to 2010," *Nature*, pp. 1–16, Mar. 2015.

[16] D. R. Feldman, W. D. Collins, S. C. Biraud, M. D. Risser, D. D. Turner, P. J. Gero, Tadić, D. Helmig, S. Xie, E. J. Mlawer, T. R. Shippert, and M. S. Torn, "Observationally derived rise in methane surface forcing mediated by water vapour trends," *Nature Geoscience*, vol. 11, no. 4, pp. 238–243, Apr. 2018.

[17] M. D. Shupe, D. D. Turner, V. P. Walden, R. Bennartz, M. P. Cadeddu, B. B. Castellani, C. J. Cox, D. R. Hudak, M. S. Kulie, N. B. Miller, R. R. I. Neely, W. D. Neff, and P. M. Rowe, "High and Dry: New Observations of Tropospheric and Cloud Properties above the Greenland Ice Sheet," *Bull. Amer. Meteor. Soc.*, vol. 94, pp. 169–186, Feb. 2013.

[18] J. Hsu and M. J. Prather, "Stratospheric variability and tropospheric ozone," *J. Geophys. Res.*, vol. 114, no. 6, pp. 179–15, Mar. 2009.

[19] P. G. Hess and R. Zbinden, "Stratospheric impact on tropospheric ozone variability and trends: 1990–2009," *Atmos. Chem. Phys.*, vol. 13, no. 2, pp. 649–674, 2013.

[20] J. L. Neu, T. Flury, G. L. Manney, M. L. Santee, N. J. Livesey, and J. Worden, "Tropospheric ozone variations governed by changes in stratospheric circulation," *Nature Geoscience*, vol. 7, no. 5, pp. 340–344, Apr. 2014.

[21] N. R. P. Harris, B. Hassler, F. Tummon, G. E. Bodeker, D. Hubert, I. Petropavlovskikh, W. Steinbrecht, J. Anderson, P. K. Bhartia, C. D. Boone, A. Bourassa, S. M. Davis, D. Degenstein, A. Delcloo, S. M. Frith, L. Froidevaux, S. Godin-Beekmann, N. Jones, M. J. Kurylo, E. Kyrölä, M. Laine, S. T. Leblanc, J. C. Lambert, B. Liley, E. Mahieu, A. Maycock, M. De Mazière, A. Parrish, R. Querel, K. H. Rosenlof, C. Roth, C. Sioris, J. Staehelin, R. S. Stolarski, R. Stübi, J. Tamminen, C. Vigouroux, K. A. Walker, H. J. Wang, J. Wild, and J. M. Zawodny, "Past changes in the vertical distribution of ozone – Part 3: Analysis and interpretation of trends," *Atmos. Chem. Phys.*, vol. 15, no. 17, pp. 9965–9982, 2015.

[22] S. Bahramvash-Shams, V. P. Walden, I. Petropavlovskikh, D. Tarasick, R. Kivi, S. Oltmans, B. Johnson, P. Cullis, C. W. Sterling, L. Thölix, and Q. Errera, "Variations in the vertical profile of ozone at four high-latitude Arctic sites from 2005 to 2017," *Atmos. Chem. Phys.*, vol. 19, no. 15, pp. 9733–9751, 2019.

[23] M. Shangguan, W. Wang, and S. Jin, "Variability of temperature and ozone in the upper troposphere and lower stratosphere from multi-satellite observations and reanalysis data," *Atmos. Chem. Phys.*, vol. 19, no. 10, pp. 6659–6679, 2019.

[24] J. D. Haigh, "The role of stratospheric ozone in modulating the solar radiative forcing of climate," *Nature*, vol. 370, no. 6, pp. 544–546, Aug. 1994.

[25] V. Ramaswamy, M. D. Schwarzkopf, and W. J. Randel, "Fingerprint of ozone depletion in the spatial and temporal pattern of recent lower-stratospheric cooling," *Nature*, vol. 382, no. 6, pp. 616–618, Aug. 1996.

[26] P. J. Nowack, N. Luke Abraham, A. C. Maycock, P. Braesicke, J. M. Gregory, M. M. Joshi, A. Osprey, and J. A. Pyle, "A large ozone-circulation feedback and its implications for global warming assessments," *Nature Clim Change*, vol. 5, no. 1, pp. 41–45, 2015.

[27] N. Calvo, L. M. Polvani, and S. Solomon, "On the surface impact of Arctic stratospheric ozone extremes," *Environ. Res. Lett.*, vol. 10, no. 9, pp. 094003–9, Sep. 2015.

[28] E. Romanowsky, D. X. R. Handorf, R. Jaiser, I. Wohltmann, W. Dorn, J. Ukita, J. Cohen, K. Dethloff, and M. Rex, "The role of stratospheric ozone for Arctic-midlatitude linkages," *Scientific Reports*, vol. 9, no. 1, pp. 1–7, May 2019.

[29] M. P. Baldwin and T. J. Dunkerton, "Stratospheric Harbingers of Anomalous Weather Regimes," *Science*, vol. 294, no. 5, pp. 581–584, Oct. 2001.

[30] S. Ineson and A. A. Scaife, "The role of the stratosphere in the European climate response to El Niño," *Nature Geoscience*, vol. 2, no. 1, pp. 32–36, Dec. 2008.

[31] A. Y. Karpechko, J. Perlwitz, and E. Manzini, "A model study of tropospheric impacts of the Arctic ozone depletion 2011," *J. Geophys. Res.*, vol. 119, no. 1, pp. 7999–8014, Jul. 2014.

[32] F. Xie, J. Li, W. Tian, Q. Fu, F.-F. Jin, Y. Hu, J. Zhang, W. Wang, C. Sun, J. Feng, Y. Yang, and R. Ding, "A connection from Arctic stratospheric ozone to El Niño-Southern oscillation," *Environ. Res. Lett.*, vol. 11, no. 12, pp. 124026–12, Dec. 2016.

[33] C. Cagnazzo and E. Manzini, "Impact of the Stratosphere on the Winter Tropospheric Teleconnections between ENSO and the North Atlantic and European Region," *J. Climate*, vol. 22, no. 5, pp. 1223–1238, Mar. 2009.

[34] G. Ancellet, N. Daskalakis, J. C. Raut, D. Tarasick, J. Hair, B. Quennehen, F. Ravetta, H. Schlager, A. J. Weinheimer, A. M. Thompson, B. Johnson, J. L. Thomas, and K. S. Law, "Analysis of the latitudinal variability of tropospheric ozone in the Arctic using the large number of aircraft and ozonesonde observations in early summer 2008," *Atmos. Chem. Phys.*, vol. 16, no. 20, pp. 13341–13358, 2016.

[35] C. Wespes, L. Emmons, D. P. Edwards, J. Hannigan, D. Hurtmans, M. Saunois, P. F. Coheur, C. Clerbaux, M. T. Coffey, R. L. Batchelor, R. Lindenmaier, K. Strong, A. J. Weinheimer, J. B. Nowak, T. B. Ryerson, J. D. Crounse, and P. O. Wennberg, "Analysis of ozone and nitric acid in spring and summer Arctic pollution using aircraft, ground-based, satellite observations and MOZART-4 model: source attribution and partitioning," *Atmos. Chem. Phys.*, vol. 12, no. 1, pp. 237–259, Jan. 2012.

[36] T. G. Shepherd, "Dynamics, stratospheric ozone, and climate change," *Atmosphere-Ocean*, vol. 46, no. 1, pp. 117–138, Jan. 2008.

[37] H. E. Rieder, L. M. Polvani, and S. Solomon, "Distinguishing the impacts of ozone-depleting substances and well-mixed greenhouse gases on Arctic stratospheric ozone and temperature trends," *Geophys. Res. Lett.*, vol. 41, no. 7, pp. 2652–2660, Apr. 2014.

[38] I. Petropavlovskikh, S. Godin-Beekmann, D. Hubert, R. Damadeo, B. Hassler, and V. Sofieva, "SPARC/IO3C/GAW Report on Long-term Ozone Trends and Uncertainties in the Stratosphere," SPARC/IO3C/GAW, SPARC Report No. 9, GAW Report No. 241, Feb. 2019.

[39] W. Steinbrecht, L. Froidevaux, R. Fuller, R. Wang, J. Anderson, C. Roth, A. Bourassa, D. Degenstein, R. Damadeo, J. Zawodny, S. Frith, R. McPeters, P. Bhartia, J. Wild, C. Long, S. Davis, K. Rosenlof, V. Sofieva, K. Walker, N. Rahpoe, A. Rozanov, M. Weber, A. Laeng, T. von Clarmann, G. Stiller, N. Kramarova, S. Godin-Beekmann, T. Leblanc, R. Querel, D. Swart, I. Boyd, K. Hocke, N. Kämpfer, E. Maillard Barras, L. Moreira, G. Nedoluha, C. Vigouroux, T. Blumenstock, M. Schneider, O. García, N. Jones, E. Mahieu, D. Smale, M. Kotkamp, J. Robinson, I. Petropavlovskikh, N. Harris, B. Hassler, D. Hubert, and F. Tummon, "An update on ozone profile trends for the period 2000 to 2016," *Atmos. Chem. Phys.*, vol. 17, no. 17, pp. 10675–10690, 2017.

[40] F. Tummon, B. Hassler, N. R. P. Harris, J. Staehelin, W. Steinbrecht, J. Anderson, G. E. Bodeker, A. Bourassa, S. M. Davis, D. Degenstein, S. M. Frith, L. Froidevaux, E. Kyrölä, M. Laine, C. Long, A. A. Penckwitt, C. E. Sioris, K. H. Rosenlof, C. Roth, H. J.

Wang, and J. Wild, "Intercomparison of vertically resolved merged satellite ozone data sets: interannual variability and long-term trends," *Atmos. Chem. Phys.*, vol. 15, no. 6, pp. 3021–3043, Mar. 2015.

[41] W. T. Ball, J. Alsing, D. J. Mortlock, J. Staehelin, J. D. Haigh, T. Peter, F. Tummon, R. Stubi, A. Stenke, J. Anderson, A. Bourassa, S. M. Davis, D. Degenstein, S. Frith, L. Froidevaux, C. Roth, V. Sofieva, R. Wang, J. Wild, P. Yu, J. R. Ziemke, and E. V. Rozanov, "Evidence for a continuous decline in lower stratospheric ozone offsetting ozone layer recovery," *Atmos. Chem. Phys.*, vol. 18, no. 2, pp. 1379–1394, Feb. 2018.

[42] W. T. Ball, J. Alsing, J. Staehelin, S. M. Davis, L. Froidevaux, and T. Peter, "Stratospheric ozone trends for 1985–2018: sensitivity to recent large variability," *Atmos. Chem. Phys.*, vol. 19, no. 19, pp. 12731–12748, 2019.

[43] K. Wargan, C. Orbe, S. Pawson, J. R. Ziemke, L. D. Oman, M. A. Olsen, L. Coy, and K. Emma Knowland, "Recent Decline in Extratropical Lower Stratospheric Ozone Attributed to Circulation Changes," *Geophys. Res. Lett.*, vol. 45, no. 10, pp. 5166–5176, May 2018.

[44] M. P. Chipperfield, S. Dhomse, R. Hossaini, W. Feng, M. L. Santee, M. Weber, J. P. Burrows, J. D. Wild, D. Loyola, and M. Coldewey-Egbers, "On the Cause of Recent Variations in Lower Stratospheric Ozone," *Geophys. Res. Lett.*, vol. 45, no. 11, pp. 5718–5726, Jun. 2018.

[45] M. M. Rienecker, M. J. Suárez, R. Gelaro, R. Todling, J. Bacmeister, E. Liu, M. G. Bosilovich, S. D. Schubert, L. Takacs, G.-K. Kim, S. Bloom, J. Chen, D. Collins, A. Conaty, A. da Silva, W. Gu, J. Joiner, R. D. Koster, R. Lucchesi, A. Molod, T. Owens, S. Pawson, P. Pegion, C. R. Redder, R. Reichle, F. R. Robertson, A. G. Ruddick, M. Sienkiewicz, and J. Woollen, "MERRA: NASA's Modern-Era Retrospective Analysis for Research and Applications," *J. Climate*, vol. 24, no. 14, pp. 3624–3648, Jul. 2011.

[46] R. Gelaro, W. McCarty, M. J. Suárez, R. Todling, A. Molod, L. Takacs, C. A. Randles, A. Darmenov, M. G. Bosilovich, R. Reichle, K. Wargan, L. Coy, R. Cullather, C. Draper, S. Akella, V. Buchard, A. Conaty, A. M. da Silva, W. Gu, G.-K. Kim, R. Koster, R. Lucchesi, D. Merkova, J. E. Nielsen, G. Partyka, S. Pawson, W. Putman, M. Rienecker, S. D. Schubert, M. Sienkiewicz, and B. Zhao, "The Modern-Era Retrospective Analysis for Research and Applications, Version 2 (MERRA-2)," *J. Climate*, vol. 30, no. 14, pp. 5419–5454, Jul. 2017.

[47] K. Wargan, G. Labow, S. Frith, S. Pawson, N. Livesey, and G. Partyka, "Evaluation of the Ozone Fields in NASA's MERRA-2 Reanalysis," *J. Climate*, vol. 30, no. 8, pp. 2961–2988, Apr. 2017.

[48] S. Bahramvash-Shams, V. P. Walden, J. W. Hannigan, I. Petropavlovskikh, A. Butler, and A. de la Cámara, "Analyzing ozone variations and uncertainties at high latitudes during Sudden Stratospheric Warming events using MERRA-2", (under review), 2021.

[49] M. Liu and D. Hu, "Different Relationships between Arctic Oscillation and Ozone in the Stratosphere over the Arctic in January and February," *Atmosphere*, vol. 12, no. 129, pp. 129–14, Feb. 2021.

[50] S. Safieddine, M. Bouillon, A.-C. Paracho, J. Jumelet, F. Tencé, A. Pazmino, F. Goutail, C. Wespes, S. Bekki, A. Boynard, J. Hadji-Lazaro, P.-F. Coheur, D. Hurtmans, and C. Clerbaux, "Antarctic Ozone Enhancement During the 2019 Sudden Stratospheric Warming Event," *Geophys. Res. Lett.*, vol. 47, pp. 1–10, Jul. 2020.

[51] D. Spänkuch, W. Döhler, J. Güldner, and E. Schulz, "Estimation of the Amount of Tropospheric Ozone in a Cloudy Sky by Ground-Based Fourier-Transform Infrared Emission Spectroscopy," *Applied Optics LP*, vol. 37, no. 1, pp. 3133–3142, May 1998.

[52] K. J. Lightner, W. W. McMillan, K. J. McCann, R. M. Hoff, M. J. Newchurch, E. J. Hintsa, and C. D. Barnet, "Detection of a tropospheric ozone anomaly using a newly developed ozone retrieval algorithm for an up-looking infrared interferometer," *Journal of Geophysical Research*, vol. 114, no. 6304, 2009.

[53] M. Maahn, D. D. Turner, U. Löhnert, D. J. Posselt, K. Ebell, G. G. Mace, and J. M. Comstock, "Optimal Estimation Retrievals and Their Uncertainties: What Every Atmospheric Scientist Should Know," *Bull. Amer. Meteor. Soc.*, vol. 101, no. 9, pp. E1512–E1523, Sep. 2020.

[54] R. O. Knuteson, H. E. Revercomb, F. A. Best, N. C. Ciganovich, R. G. Dedecker, T. P. Dirkx, S. C. Ellington, W. F. Feltz, R. K. Garcia, H. B. Howell, W. L. Smith, J. F. Short, And D. C. Tobin , 2004, "Atmospheric emitted radiance interferometer. Part I: Instrument design," *J. Atmos. Oceanic Technol.*, vol. 21, no. 12, pp. 1763–1776, Dec. 2004.

[55] R. O. Knuteson, H. E. Revercomb, F. A. Best, N. C. Ciganovich, R. G. Dedecker, T. P. Dirkx, S. C. Ellington, W. F. Feltz, R. K. Garcia, H. B. Howell, W. L. Smith, J. F. Short, and D. C. Tobin, "Atmospheric Emitted Radiance Interferometer. Part II: Instrument Performance," *J. Atmos. Oceanic Technol.*, vol. 21, no. 12, pp. 1777–1789, 2004.

[56] D. D. Turner, E. J. Mlawer, and H. E. Revercomb, *Water vapor observations in the ARM Program,* "*The Atmospheric Radiation Measurement Program: The First 20 Years*," Bulletin of the American Meteorological Society, 2016, pp. 13.1–13.18.

[57] H. E. Revercomb, W. L. Smith, H. Buijs, H. B. Howell, and D. D. Laporte, "Radiometric calibration of IR Fourier transform spectrometers - Solution to a problem with the High-Resolution Interferometer Sounder," *Applied Optics (ISSN 0003-6935)*, vol. 27, no. 15, pp. 3210–3218, Aug. 1988.

[58] D. D. Turner, "Improved ground-based liquid water path retrievals using a combined infrared and microwave approach," *J. Geophys. Res.*, vol. 112, no. D15204, 2007.

[59] D. T. Kleist, D. F. Parrish, J. C. Derber, R. Treadon, W. Wu, and S. Lord, "Introduction of the GSI into the NCEP global data assimilation system," *Weather and Forcasting*, vol. 24, no. 6, pp. 24(6)–1691–1705.

[60] A. Molod, L. Takacs, M. Suarez, and J. Bacmeister, "Development of the GEOS-5 atmospheric general circulation model: evolution from MERRA to MERRA2," *Geosci. Model Dev.*, vol. 8, no. 5, pp. 1339–1356, 2015.

[61] W. D. Komhyr, "Operations handbook-ozone measurements to 40-km altitude with Model 4A Electrochemical Concentration Cell (ECC) ozonesonaes (used with 1680-MHz radiosondes)", Sep. 1986.

[62] W. D. Komhyr, R. D. Grass, and R. K. Leonard, "Dobson spectrophotometer 83: A standard for total ozone measurements, 1962–1987," *J. Geophys. Res.*, vol. 94, no. 7, pp. 9847–9861, Jul. 1989.

[63] T. Deshler, J. L. Mercer, H. G. J. Smit, R. Stubi, G. Levrat, B. J. Johnson, S. J. Oltmans, R. Kivi, A. M. Thompson, J. Witte, J. Davies, F. J. Schmidlin, G. Brothers, and T. Sasaki, "Atmospheric comparison of electrochemical cell ozonesondes from different manufacturers, and with different cathode solution strengths: The Balloon Experiment on Standards for Ozonesondes," *J. Geophys. Res.*, vol. 113, no. D, p. D04307, Feb. 2008.

[64] T. Deshler, R. Stubi, F. J. Schmidlin, J. L. Mercer, H. G. J. Smit, B. J. Johnson, R. Kivi, and B. Nardi, "Methods to homogenize electrochemical concentration cell (ECC) ozonesonde measurements across changes in sensing solution concentration or ozonesonde manufacturer," *Atmos. Meas. Tech.*, vol. 10, no. 6, pp. 2021–2043, Jun. 2017.

[65] C. Vigouroux, M. De Mazière, P. Demoulin, C. Servais, F. Hase, T. Blumenstock, I. Kramer, M. Schneider, J. Mellqvist, A. Strandberg, V. Velazco, J. Notholt, R. Sussmann, W. Stremme, A. Rockmann, T. Gardiner, M. Coleman, and P. Woods, "Evaluation of tropospheric and stratospheric ozone trends over Western Europe from ground-based FTIR network observations," *Atmos. Chem. Phys.*, vol. 8, no. 23, pp. 6865–6886, 2008.

[66] M. K. McDonald, D. N. Turnbull, and D. P. Donovan, "Steller Brewer, ozonesonde, and DIAL measurements of Arctic O3 column over Eureka, N.W.T. during 1996 winter/spring," *Geophys. Res. Lett.*, vol. 26, no. 15, pp. 2383–2386, Aug. 1999.

[67] J. A. Logan, "Trends in the vertical distribution of ozone: An analysis of ozonesonde data," *J. Geophys. Res.*, vol. 99, no. D, pp. 25–, Dec. 1994.

[68] J. A. Logan, I. A. Megretskaia, A. J. Miller, G. C. Tiao, D. Choi, L. Zhang, R. S. Stolarski, G. J. Labow, S. M. Hollandsworth, G. E. Bodeker, H. Claude, D. de Muer, J. B. Kerr, D. W. Tarasick, S. J. Oltmans, B. Johnson, F. Schmidlin, J. Staehelin, P. Viatte, and O. Uchino, "Trends in the vertical distribution of ozone: A comparison of two analyses of ozonesonde data," *J. Geophys. Res.*, vol. 104, no. D, pp. 26–, Nov. 1999.

[69] R. S. Stolarski, "History of the Study of Atmospheric Ozone," *Ozone Science Engineering*, vol. 23, no. 6, pp. 421–428, 2001.

[70] A. Gaudel, G. Ancellet, and S. Godin-Beekmann, "Analysis of 20 Years of tropospheric ozone vertical profiles by lidar and ecc at observatoire de Haute Provence (OHP) at 44–N, 6.7–E," *Atmospheric Environment*, vol. 113, no. C, pp. 78–89, Jul. 2015.

[71] C. W. Sterling, B. J. Johnson, S. J. Oltmans, H. G. J. Smit, A. F. Jordan, P. D. Cullis, E. G. Hall, A. M. Thompson, and J. C. Witte, "Homogenizing and Estimating the Uncertainty in NOAA's Long Term Vertical Ozone Profile Records Measured with the Electrochemical Concentration Cell Ozonesonde," *Atmos. Meas. Tech. Discuss.*, pp. 1–39, Dec. 2017.

[72] C. D. Rodgers, "Retrieval of atmospheric temperature and composition from remote measurements of thermal radiation," *Reviews of Geophysics*, vol. 14, no. 4, pp. 609–624, Jan. 1976.

[73] C. D. Rodgers, *Inverse Methods for Atmospheric Sounding - Theory and Practice*, vol. 2. World Scientific Publishing Co. Pte. Ltd., 2000.

[74] J. W. Hannigan, M. T. Coffey, and A. Goldman, "Semiautonomous FTS Observation System for Remote Sensing of Stratospheric and Tropospheric Gases," *J. Atmos. Oceanic Technol.*, vol. 26, no. 9, pp. 1814–1828, Sep. 2009.

[75] C. Vigouroux, T. Blumenstock, M. Coffey, Q. Errera, O. García, N. B. Jones, J. W. Hannigan, F. Hase, B. Liley, E. Mahieu, J. Mellqvist, J. Notholt, M. Palm, G. Persson, M. Schneider, C. Servais, D. Smale, L. Thölix, and M. De Mazière, "Trends of ozone total columns and vertical distribution from FTIR observations at eight NDACC stations around the globe," *Atmos. Chem. Phys.*, vol. 15, no. 6, pp. 2915–2933, 2015.

[76] B. Barret, M. De Mazière, and P. Demoulin, "Retrieval and characterization of ozone profiles from solar infrared spectra at the Jungfraujoch," *Journal of Geophysical Research*, vol. 107, no. 24, p. 4788, 2002.

[77] L. S. Rothman, I. E. Gordon, A. Barbe, D. C. Benner, P. F. Bernath, M. Birk, V. Boudon, L. R. Brown, A. Campargue, J. P. Champion, K. Chance, L. H. Coudert, V. Dana, V. M. Devi, S. Fally, J. M. Flaud, R. R. Gamache, A. Goldman, D. Jacquemart, I. Kleiner, N. Lacome, W. J. Lafferty, J. Y. Mandin, S. T. Massie, S. N. Mikhailenko, C. E. Miller, N. Moazzen-Ahmadi, O. V. Naumenko, A. V. Nikitin, J. Orphal, V. I. Perevalov, A. Perrin, A. Predoi-Cross, C. P. Rinsland, M. Rotger, M. Šimečková, M. A. H. Smith, K. Sung, S. A. Tashkun, J. Tennyson, R. A. Toth, A. C. Vandaele, and J. Vander Auwera, "The HITRAN 2008 molecular spectroscopic database," *Journal of Quantitative Spectroscopy and Radiative Transfer*, vol. 110, no. 9, pp. 533–572, Jun. 2009.

[78] D. R. Marsh, M. J. Mills, D. E. Kinnison, J.-F. Lamarque, N. Calvo, and L. M. Polvani, "Climate Change from 1850 to 2005 Simulated in CESM1(WACCM)," *J. Climate*, vol. 26, no. 19, pp. 7372–7391, Oct. 2013.

[79] M. A. H. Smith, V. M. Devi, D. C. Benner, and C. P. Rinsland, "Absolute intensities of 16O3 lines in the 9-11 μm region," *J. Geophys. Res.*, vol. 106, no. D, pp. 9909–9921, May 2001.

[80] C. D. Rodgers and B. J. Connor, "Intercomparison of remote sounding instruments," *J. Geophys. Res.*, vol. 108, no. 3, pp. n/a–n/a, Feb. 2003.